Enhanced Ammonia Sensing with $MAPbBr_3$ Perovskite and (R/S)-OBN-tCz: A Study on Sensitivity and Stability Improvements

Chang Zhang[a], Xin Zhang[a]*, Wei Wang[a], Hao Xue[a], Qian He[a], Fenglin Li[a], Xiaoli Wang[a], Qinghui Jin[a], Kun Zhou[b]*, Jiawen Jian[a]

[a] Faculty of electrical engineering and computer science, Ningbo University, 818 Fenghua Road, Ningbo, 315211, China
[b] Department of Chemistry, The Hong Kong University of Science and Technology, Kowloon 100071 Hong Kong, China.

Corresponding Authors

*Email: Xin Zhang: zhangxin1@nbu.edu.cn
Kun Zhou: kunzhouzk@gmail.com

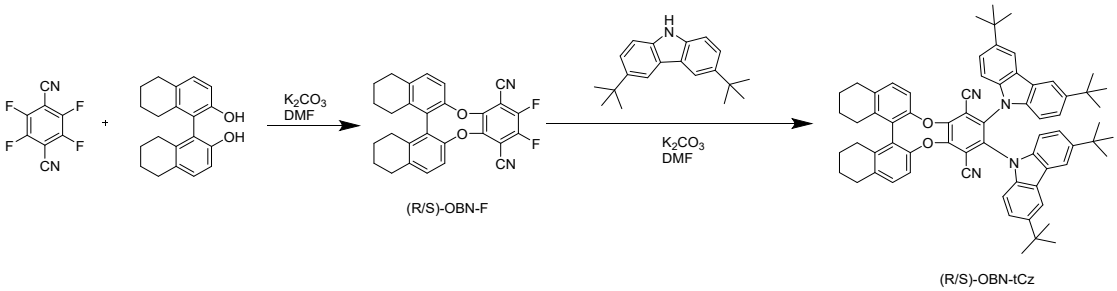

Scheme S1. Chemical synthesis pathway for (R/S)-OBN-tCz.

(R/S)-(-)-5,5′,6,6′,7,7′,8,8′-octahydro-1,1′-bi-2-naphthol ((R/S)-OBN) is located on the left side of the molecule, imparting its chiral characteristics, which allow the molecule to exist as two mirror-image isomers (R and S forms). The central ring structure is derived from tetrafluoroterephthalonitrile, while the carbazole (Cz) part is situated on the right side, connected to the central ring via a nitrogen atom. The molecular structure includes two cyano (CN) groups. The molecular structure includes two cyano (CN) groups, with nitrogen atoms containing lone pairs of electrons, giving them Lewis base properties that enable interaction with uncoordinated Pb^{2+} ions (Lewis acids). The conjugated system within the molecule aids in distributing electron density, enhancing its stability, and providing more reactive sites for interactions with perovskite surface defects.

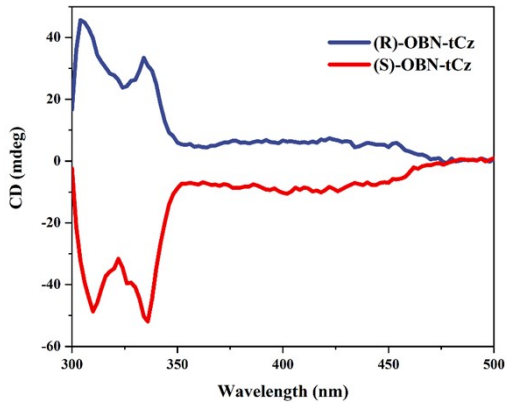

Figure S2. CD spectra of (R/S)-OBN-tCz in toluene (5.0×10^{-5} M).

The different chirality of materials exhibits differences in the interaction with left-hand circularly polarized (LCP) and right-hand circularly polarized (RCP) light when excited by light. As illustrated in Fig.S2, the CD spectra of (R)-OBN-Cz and (S)-OBN-Cz display an obvious mirror-image relationship. The strong Cotton effects in short wavelength region around 300 nm could be assigned to the characteristic absorption of chiral (R/S)-octahydro-binaphthol (OBN) unit. Meanwhile, the Cotton effects with the maximum band around 400 nm are assigned to the absorption of the donor (D)–acceptor

(A) electronic structure of Thermally activated delayed fluorescence (TADF) unit, indicating that the chirality is successfully induced into the TADF skeleton through chirality transmitting of OBN unit in the ground state.

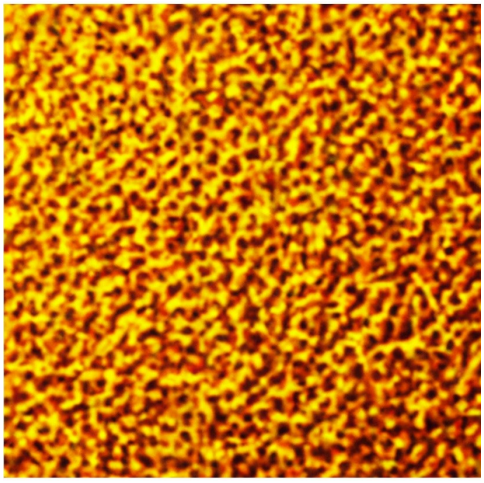

Figure S3. The micro-morphology of the perovskite $MAPbBr_3$ surface captured by Atomic Force Microscopy (AFM).

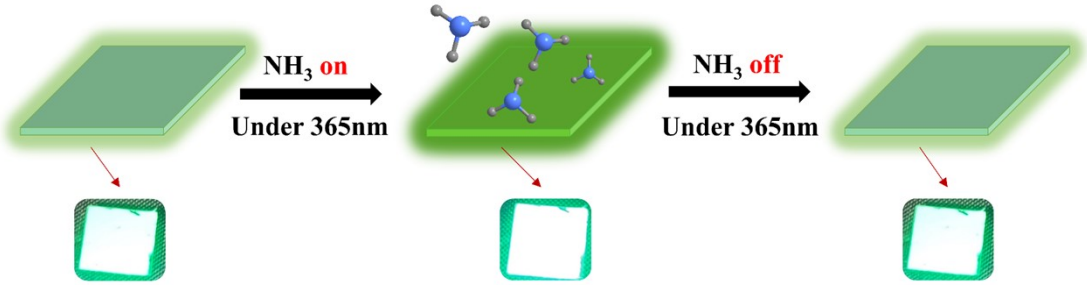

Figure S4. Visual changes of the sensor in air and exposure to ammonia gas.

The regression **Equation S5** when doped with different levels of (R)-OBN-tCz is:

0 mg R: $(F-F_0)/F_0 = 0.13529C - 0.10329$

0.25 mg R: $(F-F_0)/F_0 = 0.16968C - 0.11261$

0.5 mg R: $(F-F_0)/F_0 = 0.13943C - 0.06043$

The regression **Equation S6** when doped with different levels of (S)-OBN-tCz is:

0 mg S: $(F-F_0)/F_0 = 0.13361C - 0.09814$

0.25 mg S: $(F-F_0)/F_0 = 0.14114C - 0.07214$

0.5 mg S: $(F-F_0)/F_0 = 0.16607C - 0.138$

The fluorescence intensity before exposure is represented by F_0, while F represents the fluorescence intensity after exposure for a specific time. C denotes the concentration value of ammonia gas.

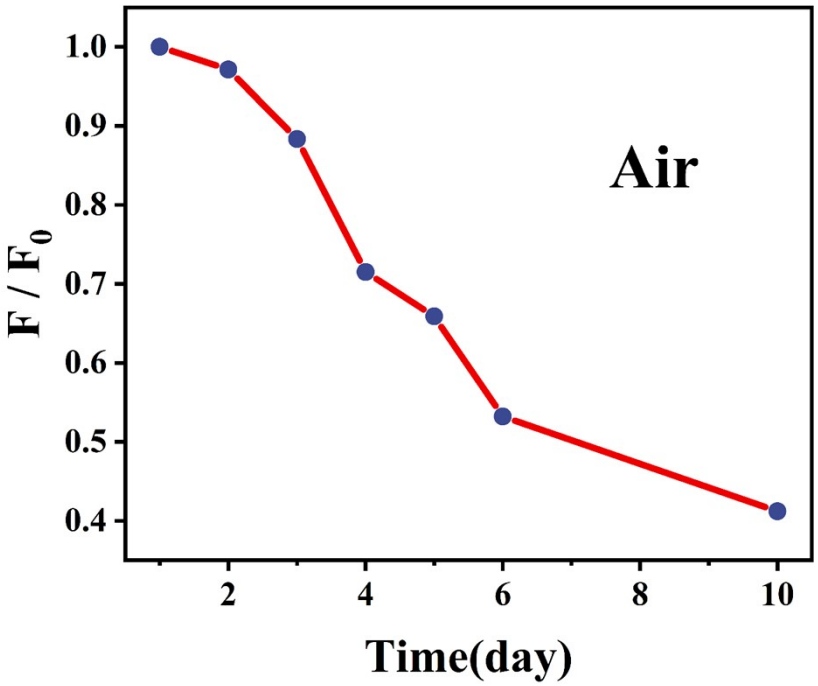

Figure S7. Changes in the performance of $MAPbBr_3$ in air.

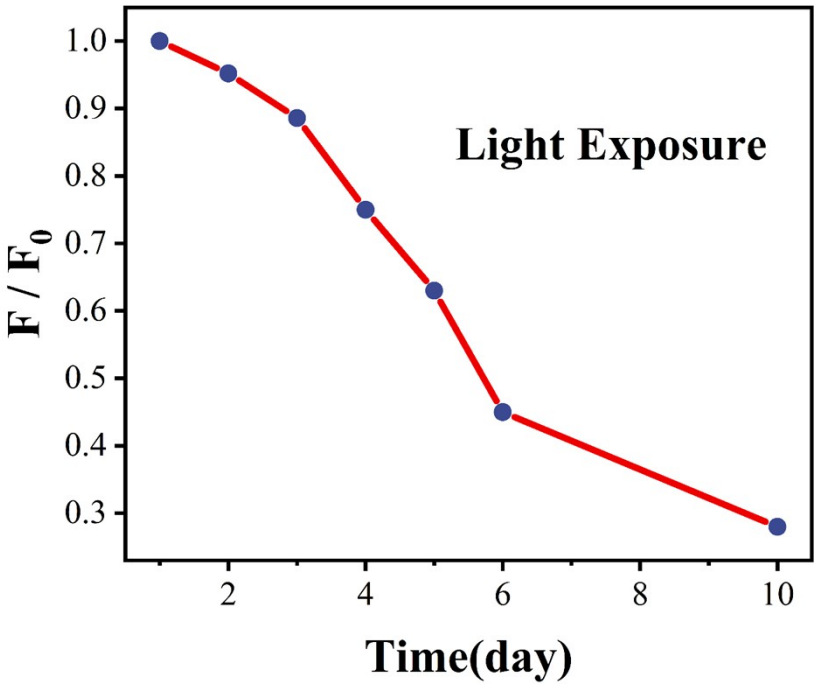

Figure S8. Changes in the performance of $MAPbBr_3$ in light exposure.

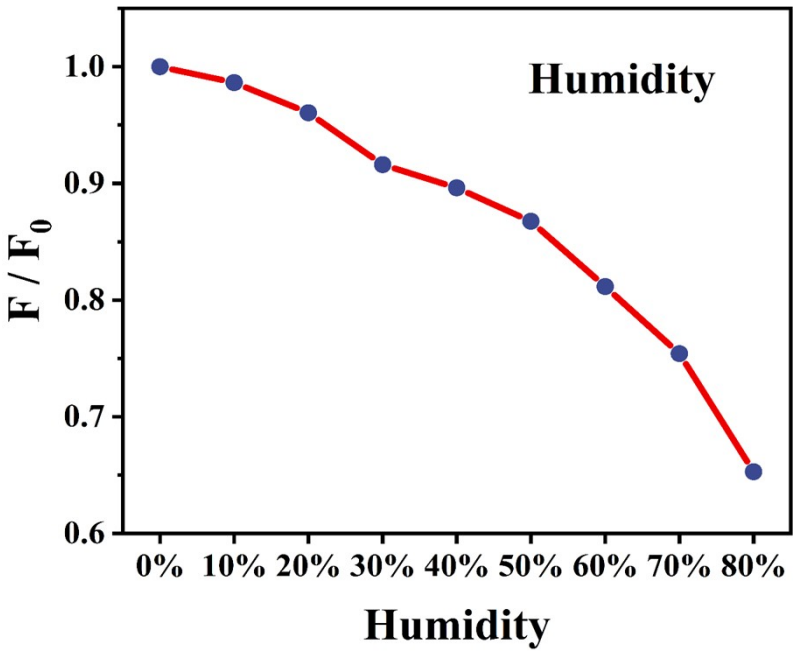

Figure S9. Display the changes in the $MAPbBr_3$ photoluminescent capability under varying levels of relative humidity.

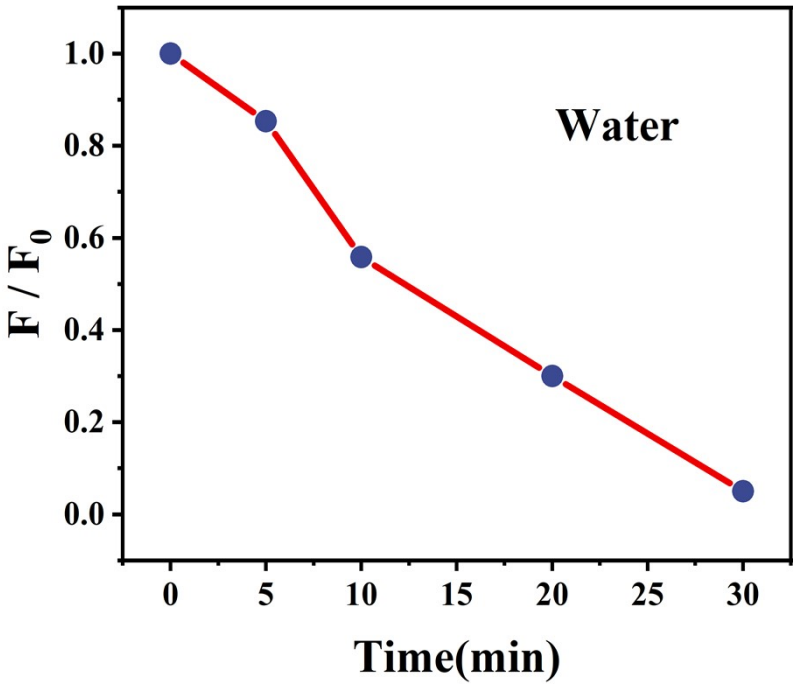

Figure S10. Changes in the properties of $MAPbBr_3$ immersed in water.

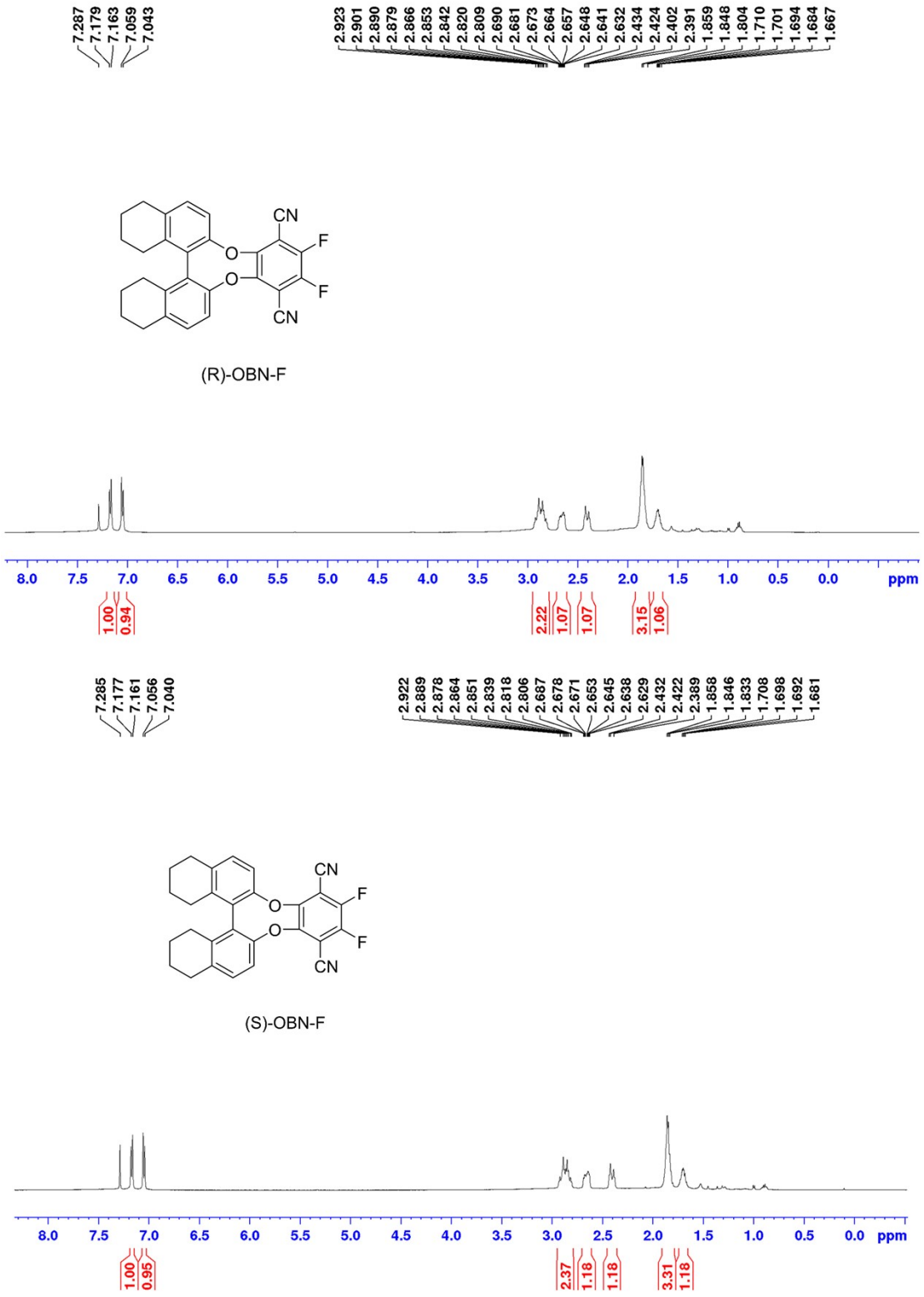

Figure S11. The ^{1}H nuclear magnetic resonance (^{1}H NMR) spectrum of (R/S)-OBN-F, with the molecular structure of (R/S)-OBN-F depicted in the inset.

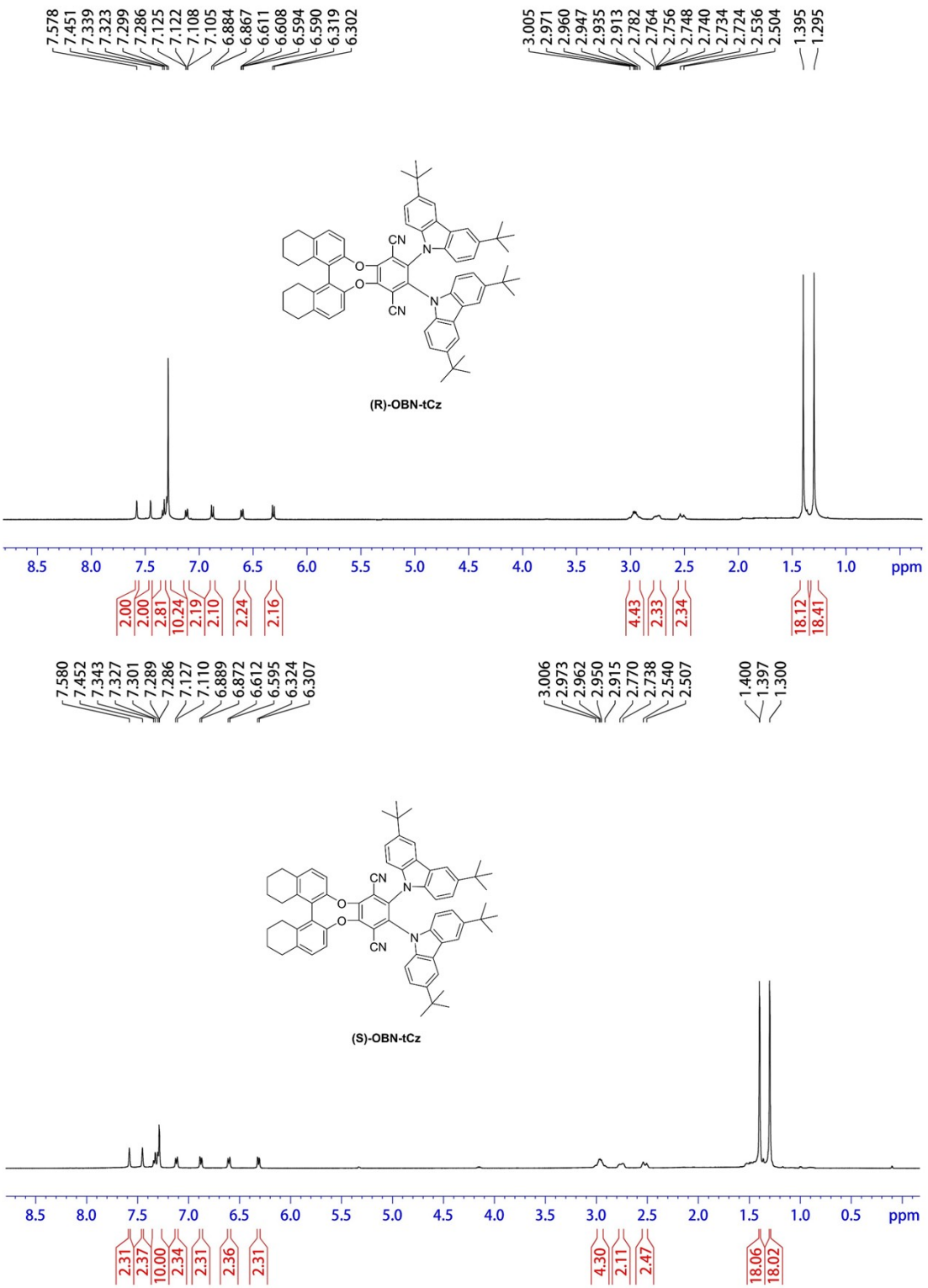

Figure S12. The ^{1}H nuclear magnetic resonance (^{1}H NMR) spectrum of (R/S)-OBN-tCz, along with its corresponding molecular structure.

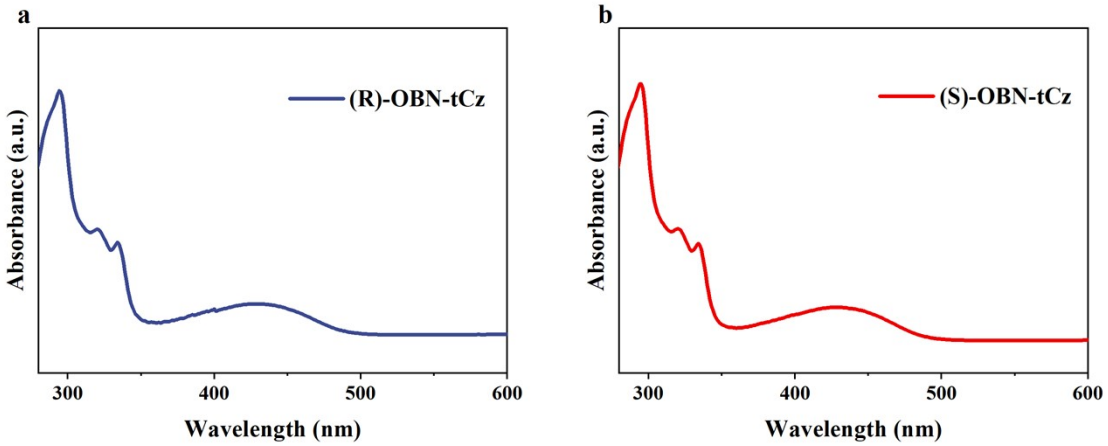

Figure S13. UV-Visible absorption spectra of (R)-OBN-tCz and (S)-OBN-tCz.

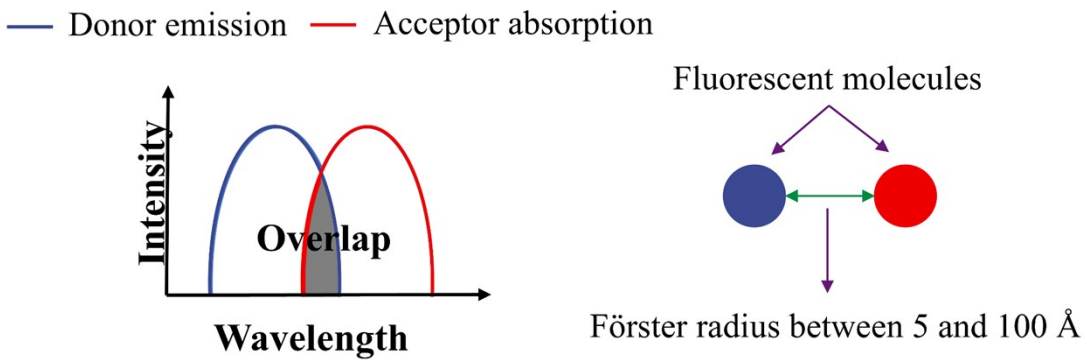

Figure S14. Illustrates the schematic of Förster Resonance Energy Transfer (FRET).

FRET occurs when the emission spectrum of the donor overlaps with the absorption spectrum of the acceptor, and Förster radius between 5 and 100 Å. Förster radius (R_0) was calculated from the following **Equation S15**:

$$R_0 = 0.211 \times \sqrt[6]{k^2 n^{-4} \Phi_D J}(\text{Å})$$

$\Phi_D$represents the quantum yield of the donor (R/S)-OBN-tCz, n refers to the refractive index of the medium surrounding the fluorophore, k represents the orientation factor of the molecular dipoles (typically k^2=2/3), and J signifies the overlap integral between the donor's emission and the acceptor's absorption. The results show that the Förster radius R_0 is 30.1 Å, indicating that the interaction between (R/S)-OBN-tCz and $MAPbBr_3$ meets the key requirements for a typical FRET process, with an energy

transfer radius within the optimal range of 5 to 100 Å.

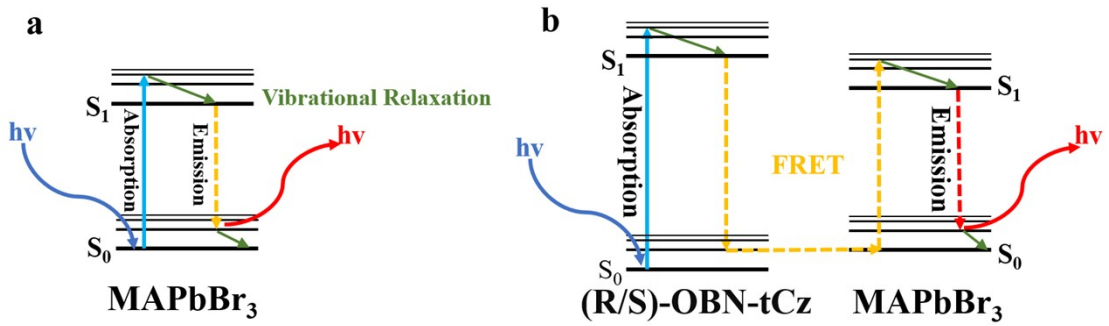

Figure S16 illustrates the fundamental principles of fluorescence and Förster Resonance Energy Transfer (FRET).

(a) illustrates how $MAPbBr_3$ absorbs photons, promoting electrons from the ground state (S_0) to the excited state (S_1). In this state, electrons may occupy various vibrational levels, typically losing energy through vibrational relaxation. As the excited state is unstable, electrons return to the ground state within nanoseconds, emitting photons with longer wavelengths (and thus lower energy) than those absorbed. (b) shows the process where the energy released by the donor molecule (R/S)-OBN-tCz during relaxation is absorbed by the acceptor $MAPbBr_3$. This absorption excites the electrons in $MAPbBr_3$, enhancing the photon emission of the acceptor.

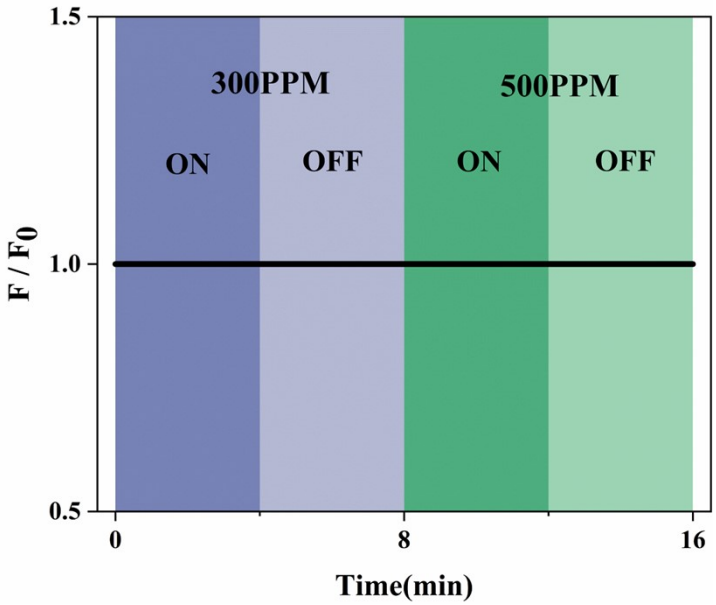

Figure S17. Depicted the fluorescent change of (R/S)-OBN-tCz and PMMA thin film when it went through 300ppm and 500ppm NH_3 gas. "ON" refers to the process of the (R/S)-OBN-tCz and PMMA being exposed to and responding to NH_3 gas, while "OFF" represents the process of the

NH_3 gas dissipating.

Limit of detection (LOD) refers to the minimum ammonia concentration that the sensor can reliably detect, which is typically calculated using the following formula:

$$LOD = \frac{3S}{K}$$

where S represents the standard deviation of the blank signal, reflecting the background noise level of the system under ammonia-free conditions, and K is the sensitivity of the sensor, defined as the slope of the linear relationship between the fluorescence signal and the ammonia concentration.

In our experiments, to obtain accurate background noise data, we repeatedly measured the fluorescence signal of the sensor under ammonia-free conditions and calculated the value of S using the standard deviation formula:

$$S = \sqrt{\frac{1}{n-1}\sum_{i=1}^{n}(x_i - \bar{x})^2}$$

where x_i represents the signal value of each measurement, $\bar{x}$ is the mean of the measured signals, and n is the number of measurements (20 times). Through statistical analysis of the experimental data (see Table S1), we obtained the standard deviation of the blank signal, S = 0.01978.

We selected the regression results with the highest sensitivity from the experiments (Equations S5 and S6), specifically when doping with 0.25 mg (R)-OBN-tCz, where the slope K =0.16968. Using the formula, we ultimately calculated the LOD of the sensor to be 0.35 ppm.

0.0032	-0.0247	0.0190	-0.0165	0.0211
-0.0159	0.0073	-0.0173	-0.0168	0.0134
0.0089	0.0017	-0.0106	-0.0192	0.0158
-0.0219	-0.0175	-0.0024	0.0083	0.0201

Table S1. Blank Signal Data

Materials	Sensing principle	LOD	Response time	Ref.
$MAPbBr_3$@PMMA	Fluorescence quenching	NM	1000 s	1
$MAPbBr_3$&TBA@GeO_2	Fluorescence quenching	0.46 ppm	61 s	2
$CsPbBr_3$@BNNF	Fluorescence quenching	NM	8 s	3
$CsPbBr_3$	Fluorescence enhancement	8.8 ppm	10 s	4
$MAPbBr_3$@mp-TiO_2	Fluorescence enhancement	0.92 ppm	7 s	5
$CsPbBr_3$@ZIF-8	Fluorescence enhancement	16 ppm	NM	6
$MAPbBr_3$&(R/S)-OBN-tCz@PMMA	Fluorescence enhancement	0.35 ppm	180 s	This work

Table S2. Summary of perovskite-based sensors optical sensors for ammonia (NM: not mentioned). Poly (methyl methacrylate) (PMMA), tetrabutylammonium (TBA), boron nitride nanofibers (BNNF), mesoporous TiO_2 (mp-TiO_2), Zeolite imidazolate framework-8 (ZIF-8).

References

1.A. K. Singh, S. Singh, V. N. Singh, G. Gupta and B. K. Gupta, *J. Colloid Interface Sci.*, 2019, **554**, 668-673.

2.G. Li, W. Zhang, C. She, S. Jia, S. Liu, F. Yue, C. Jing, Y. Cheng and J. Chu, *J. Alloys Compd.*, 2020, **835**, DOI: 10.1016/j.jallcom.2020.155386.

3.X. He, C. Yu, M. Yu, J. Lin, Q. Li, Y. Fang, Z. Liu, Y. Xue, Y. Huang and C. Tang, *Inorg. Chem.*, 2020, **59**, 1234-1241.

4.H. Huang, M. Hao, Y. Song, S. Dang, X. Liu and Q. Dong, *Small*, 2020, **16**, DOI: 10.1002/smll.201904462.

5.G. Li, C. She, Y. Zhang, H. Li, S. Liu, F. Yue, C. Jing, Y. Cheng and J. Chu, *Sens. Actuators, B*, 2021, **327**, DOI: 10.1016/j.snb.2020.128918.

6.I. Ahmad, M. Abohashrh, A. Rahim, S. Ahmad, T. Muhmood and H. Wen, *Spectrochim. Acta, Part A*, 2023, **302**, DOI: 10.1016/j.saa.2023.123091.